

# How Silver Grows on the Silicon (001) Surface: A Theoretical and Experimental Investigation

William S. Huxter,<sup>†</sup> Kai Huang,<sup>†,‡</sup> Jun Nogami,<sup>†</sup> and Chandra Veer Singh<sup>\*,†,§</sup>

<sup>†</sup>Department of Materials Science and Engineering, University of Toronto, 184 College Street, Toronto, Ontario M5S 3E4, Canada

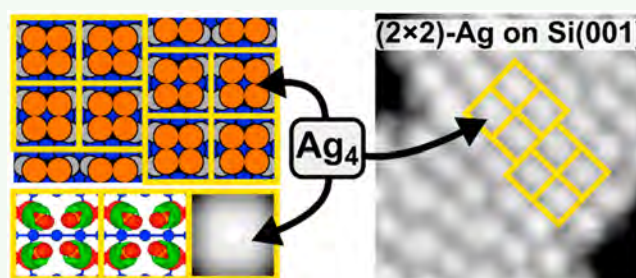
<sup>‡</sup>Guangdong Technion Israel Institute of Technology, 241 Daxue Road, Shantou, Guangdong Province 515603, P. R. China

<sup>§</sup>Department of Mechanical and Industrial Engineering, University of Toronto, 5 King's College Road, Toronto, Ontario M5S 3G8, Canada

## Supporting Information

**ABSTRACT:** When a silver film is grown on the Si(001) surface at room temperature, it forms a monolayer density film with a  $(2 \times 2)$  periodicity. Previous models of this  $(2 \times 2)$  surface, simulated by density functional theory (DFT), are found to be inconsistent with experimental observations. The DFT simulations provide evidence that a new model, the square tetramer model, describes the structure of the observed  $(2 \times 2)$ -Ag phase and is fully consistent with scanning tunneling microscopy data. Theoretical evidence of a covalent bond shared between the Ag and Si is found that matches previous experiments. Interestingly, the simulations also show that the stoichiometry between Si and Ag changes with metal coverage as adsorbate–adsorbate and adsorbate–substrate interactions balance out. At low coverages, when individual Ag adatoms interact solely with Si, a two-to-one Si–Ag–Si interaction scheme is energetically preferred. At 1 monolayer, when Ag–Ag interactions must be considered, a one-to-one Si–Ag interaction scheme is preferred, as it maximizes Ag–Ag interactions.

**KEYWORDS:** density functional theory, scanning tunneling microscopy, Si(001), Ag, thin film, metal–semiconductor interface



## INTRODUCTION

Understanding the fundamental science of simple interfaces drives the improvement of electronic devices and provides insight into other more complicated interfaces. Historically, Ag grown on Si(001) has been considered a prototypical metal/semiconductor interface where there is an abrupt transition from one material to the other.<sup>1,2</sup> The Ag/Si(001) system is also a common model system for metal adsorption on silicon where there is weak interaction with the substrate.

In addition, the Ag(111) surface is an ideal weakly interacting substrate for growing silicene<sup>3,4</sup> and other two-dimensional (2D) materials like graphene<sup>5</sup> and borophene.<sup>6</sup> Therefore, the nature of the Si–Ag interaction is highly relevant to the understanding of the growth of silicene on silver and its applications in novel 2D devices, such as silicene field effect transistors.<sup>7</sup> The growth of Ag on Si(001) can also be viewed as the inverse process of growing Si on Ag. This is ironic, since the bulk of what is known about Ag growth on Si significantly predates the discovery of silicene, and yet, there is still a fundamental lack of understanding of the behavior of Ag atoms deposited on the Si(001) surface.

For instance, this lack of understanding is as fundamental as identifying the atomic Ag film structure on Si(001) at room temperature (RT). This problem persists despite numerous RT scanning tunneling microscopy (STM) studies.<sup>8–18</sup> Unlike

the intermixed reconstructions of Ag/Si(001) at elevated temperatures,<sup>11,13,14,19–23</sup> it is established that Ag deposition at RT leaves the elements separated. The first atomic layer of Ag typically grows as 2D patches with 1 monolayer (ML) of Ag atom density, i.e., one silver atom per underlying Si substrate atom (1 ML =  $6.78 \times 10^{14}$  atoms/cm<sup>2</sup>). Experimental data shows that the 1 ML Ag film forms an ordered  $(2 \times 2)$ -Ag phase.<sup>9,11,15,16</sup> Two different experimentally derived models have been proposed claiming that the  $(2 \times 2)$ -Ag phase is based on Ag dimers.<sup>11,24</sup> However, a recent low-temperature (LT)-STM study provided evidence that Ag tetramers are the fundamental unit of the  $(2 \times 2)$ -Ag phase.<sup>25</sup> As the Ag coverage surpasses 1 ML, an unwetting phenomenon occurs.<sup>15,18</sup> Ag from the 2D layer unwets from the Si(001) surface and nucleates into three-dimensional (3D) islands. The 2D to 3D transition is not currently understood. Starr et al.<sup>26</sup> have suggested that the transition can be mediated by a kinetically hindered process; however, the exact details (energetic stabilities, diffusion pathways, and rate-determining step) are not known. Since the ML structure plays a crucial

Received: November 13, 2018

Accepted: December 17, 2018

Published: December 18, 2018

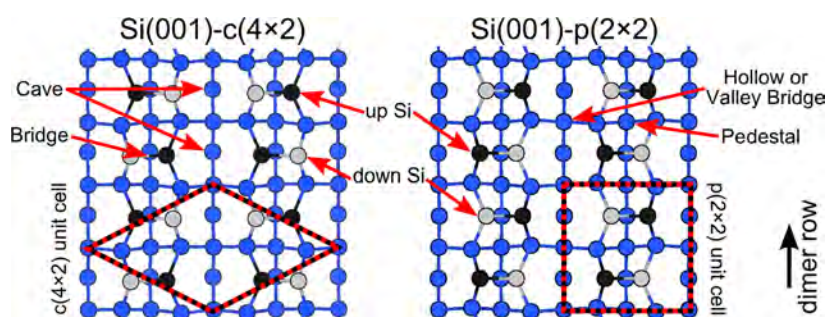


**Figure 1.** Si(001)- $c(4 \times 2)$  and Si(001)- $p(2 \times 2)$  reconstructions. Up and down Si dimer atoms are colored black and light gray, respectively. Common adsorption sites for adatoms are listed at the sides. The  $c(4 \times 2)$  and  $p(2 \times 2)$  unit cells are outlined for clarity.

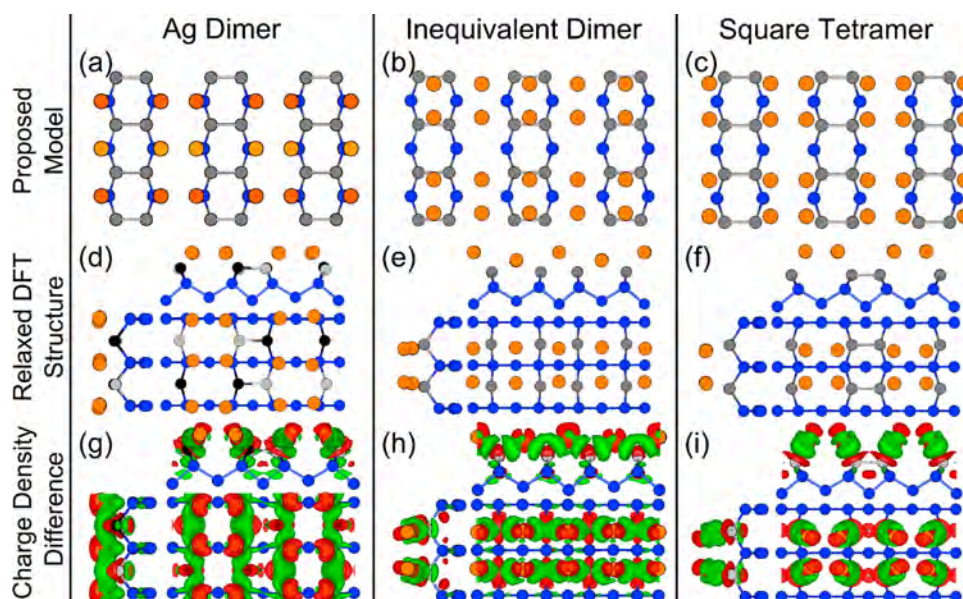


**Figure 2.** (a–c)  $(2 \times 2)$ -Ag models with two Si layers for reference, (d–f) DFT relaxed structures, and (g–i) charge density difference plots at a cut-off of  $\pm 0.002 \text{ e}/\text{\AA}^3$ . Ag atoms are orange, Si bulk atoms are blue, and Si up/down dimer atoms are black/light gray. Dimers are gray if no distinction can be made between up/down atoms. Two shades of orange are used in panel a to highlight the  $(2 \times 2)$ -Ag structure. In the charge density difference plots, green represents electron gain, and red represents electron loss.

role in understanding the unwetting process, the  $(2 \times 2)$ -Ag phase must first be understood.

To date, there is no comprehensive theoretical modeling that explores the ML structure of Ag on Si(001). Moreover, there is a general lack of theoretical studies on the Ag/Si(001) system. The density functional theory (DFT) study of Ag dimer diffusion on Si(001)- $p(2 \times 2)$  by Kong et al.<sup>27</sup> provided insight into Si–Ag interaction and provided results that agree with experiments. However, monolayer (ML) structures, as well as Ag tetramers, were not considered. Additionally, the  $p(2 \times 2)$  reconstruction is not the ground state of the Si(001) surface—the  $c(4 \times 2)$  reconstruction has a slightly lower energy,<sup>28</sup> and therefore, those Ag adsorption energies are possibly inaccurate due to different surface reconstructions. Other modeling studies of Ag on Si(001) have either studied flat Si dimers, an ideal Si(001) surface, or a different surface reconstruction<sup>22,23,29–34</sup> and therefore do not represent the type of Ag–Si interaction expected when Ag is deposited on RT Si(001).

In this paper, we use DFT and LT-STM to provide a complete description of the  $(2 \times 2)$ -Ag ML structure, starting from the Si(001)- $c(4 \times 2)$  surface. DFT relaxation performed on previously proposed atomic structure models<sup>11,24</sup> fail to

match experimental observations. The more recent model,<sup>25</sup> which features a Ag square tetramer placed in between four Si dimers, produced a structure that remains topographically consistent with experimental data. This work provides a comprehensive view of the agreement between the DFT calculations based on the new model and all aspects of the experimental STM data, including the configuration of domain boundaries in the  $(2 \times 2)$ -Ag phase and a bias dependent Ag film contrast reversal. Si–Ag interaction at 1 ML is compared to single Ag adatom adsorption in order to provide a more general picture of the growth behavior of Ag on Si(001) below 1 ML. At the same time, this system provides a clearer picture of how a metal overlayer interacts with the underlying Si reconstruction that can be relevant to the growth of metals on this technologically important surface.

## RESULTS AND DISCUSSION

**Comparison of  $(2 \times 2)$ -Ag Monolayer Models.** Before we consider the behavior of Ag on Si(001), we must briefly review the structure of the clean substrate. Si surface atoms form dimer rows to halve the number of dangling bonds. Their energy is further lowered by alternatively buckling along the row to reduce surface stress. Different buckling between rows

create the  $c(4 \times 2)$  and  $p(2 \times 2)$  reconstructions, as shown in Figure 1 along with the nomenclature for specifying common adatom adsorption sites. Experimental and theoretical techniques agree that the  $c(4 \times 2)$  reconstruction is more stable than the  $p(2 \times 2)$  reconstruction.<sup>28,35,36</sup> Complicating this issue is the fact that the buckled Si dimers flip back and forth at RT. This accounts for the  $2 \times 1$  periodicity that is seen by both LEED and STM.<sup>35</sup>

At low coverages ( $\Theta_{\text{Ag}} \ll 1$ ), the buckled Si dimers act as reaction sites.<sup>37,38</sup> Down dimer atoms have an empty  $\pi^*$ -like dangling bond state, and up dimers have a fully occupied  $\pi$ -like dangling bond state. STM studies<sup>8,11–14</sup> and theoretical modeling<sup>27</sup> for Ag in the low-coverage limit agree that the cave site, located between two Si dimers, is the most stable adsorption site. At higher coverages, however, the interaction between Ag and Si is more complex, and the question arises as to whether the Si dimers stay buckled or become more symmetric due to interactions with the Ag overlayer.

Figure 2 presents the three  $(2 \times 2)$ -Ag models along with their DFT relaxed structures and charge density difference (CDD) plots (created using eq 1). The model proposed by Lin et al.<sup>11</sup> (Figure 2a), referred to as the Ag dimer (AD) model, places Ag dimers parallel to Si dimers in the hollow site. The  $2 \times 2$  periodicity is said to originate from a buckling mechanism to reduce stress or a charge transfer mechanism on every other Ag dimer along the same Si row. The model proposed by Park et al.<sup>24</sup> (Figure 2b), referred to as the inequivalent dimer (ID) model (two inequivalent Ag dimer sites), is similar to the double layer model used to describe alkali-metal structures on Si(001),<sup>39</sup> placing Ag dimers perpendicular to the Si dimer bonds in the hollow and pedestal sites. The third model, referred to as the square tetramer (ST) model,<sup>25</sup> places four Ag atoms in a square over the hollow site with each Ag atom close to a Si dimer atom (Figure 2c). Table 1 lists adsorption

The relaxed ID structure deviates significantly from the model (Figure 2e). Ag dimers placed on top of the Si dimer row break the Si dimer bond. Additionally, the Ag–Ag bond length of  $\sim 3.1$  Å and height difference between the “up” and “down” Ag dimers of  $\sim 0.3$  Å differ from the predicted structure (Ag–Ag bond length of  $2.89 \pm 0.05$  Å and height difference of 0.57 Å).<sup>24</sup> The relaxed structure of the ST model deviates little from the initial model (Figure 2f). Si dimers sit essentially flat, and the tetramer becomes slightly rectangular with an  $\sim 0.03$  Å increase in the Ag–Ag distance perpendicular to the Si dimer bond. The Ag–Ag distances in the ST model are similar to the bulk Ag–Ag bond distance (2.89 Å). All three models show different electronic interactions. The AD and ID models show a Si–Ag–Si interaction perpendicular (Figure 2g) and parallel (Figure 2h) to the original Si dimer bond, respectively, and the ST model shows a local one-to-one Ag–Si interaction where electron density moves from both the Si and the Ag atoms into the area in between the two (Figure 2i).

Of the three models, the ID model has the most energetically stable structure, based on DFT results (calculated from eq 2 where  $E_{\text{Ag}}$  is the energy of a single Ag atom in a vacuum). The ID adsorption energy value of 2.52 eV is closest to the experimental value of 2.55 eV.<sup>26</sup> This suggests that the ID model is best candidate structure. However, angle resolved photoemission spectroscopy (ARPES) indicates that Si dimers do not break apart after RT deposition of Ag.<sup>40</sup> ARPES spectra of RT deposited Ag do not show similarities to ARPES spectra taken on the high-temperature  $(2 \times 3)$ -Ag and  $(6 \times 2)$ -Ag reconstructed surfaces where Si dimer breaking is believed to occur.<sup>41,42</sup> This implies that the basis of the ID model is unphysical—Ag dimers do not sit atop the Si dimer row at 1 ML. Furthermore, given that the energy to break a Si–Si bond is on the order of 2 eV,<sup>28</sup> it is highly unlikely that deposition of Ag would break Si dimer bonds.

$$E_{\text{ML/Ag}} = -(E_{\text{AgML+Si(001)}} - E_{\text{Si(001)}} - N_{\text{Ag}}E_{\text{Ag}})/N_{\text{Ag}} \quad (2)$$

To further investigate the three proposed models, STM images were simulated at filled- and empty-state biases. STM simulations, based on the Tersoff–Hamann theory,<sup>43</sup> and sub-ML experimental STM images are shown in Figure 3. The registration of Ag features with respect to the adjacent Si features allows for the determination of the locations of the STM maxima and minima of the  $(2 \times 2)$ -Ag phase relative to the Si dimers underneath. All models show some type of local  $2 \times 2$  character at certain biases in the simulated images. However, only the ST model correctly predicts the location of the Ag maxima and minima at all biases. The AD model (Figure 3a) places maxima over every single hollow site, and the ID model (Figure 3b) places maxima over pedestal and bridge sites. For this reason, these two models can be considered incorrect. The oval/circular maxima in the ST model (Figure 3c) are centered in every other hollow site—exactly where the STM maxima are located (Figure 3e,f).

**Domain Boundaries and Disorder in the Si(001)-Ag( $2 \times 2$ ) Structure.** More support for the ST model arises when its additional features are explored. The ST model contains an equivalent tetramer adsorption site if the model is shifted by half of its unit cell along the dimer row. This symmetry explains local checkboard patterns, a common type of disorder observed in STM images between two  $(2 \times 2)$ -Ag domains. STM simulations of this shifted structure are shown in Figure 3d. A specific example of this defect is shown in Figure 4 where a model is shown next to a corresponding STM image. The

**Table 1.** DFT Relaxed Values across  $(2 \times 2)$ -Ag ML Models Starting from the Si(001)- $c(4 \times 2)$  Reconstruction

	Si(001)- $c(4 \times 2)$	Ag dimer model	inequivalent dimer model	square tetramer model
$E_{\text{ML/Ag}}$ (eV/Ag)	--	2.37	2.52	2.43
$d_{\text{Si-Si}}$ (Å)	2.36	2.47	3.28	2.44
$d_{\text{Si-Ag}}$ (Å)	--	2.65	2.46	2.44
		2.58		
$d_{\text{Ag-Ag}}$ (Å)	--	3.00	3.1	2.81
				2.84
$\theta_{\text{Si-Si}}$ (deg)	19.4	2.5	--	0.61
$\theta_{\text{Ag-Si}}$ (deg)	--	51	41.5	59.4
			32.3	

energies, bond lengths, and relevant angles taken with respect to the surface plane. Results presented were obtained on a Si(001)- $c(4 \times 2)$  substrate. Little to no deviation was found on the  $p(2 \times 2)$  reconstruction. (See section S1 of the Supporting Information for details.)

$$\Delta\rho = \rho_{\text{Ag/Si(001)}} - \rho_{\text{Ag}} - \rho_{\text{Si(001)}} \quad (1)$$

The Si dimers in the relaxed AD structure remain slightly buckled with Ag atoms preferring to sit closer to the down Si dimer atoms (Figure 2d). Relaxed Ag dimers do not alternate in height, and a  $2 \times 2$  periodicity never develops even when an initial height difference is included to induce a  $2 \times 2$  structure.

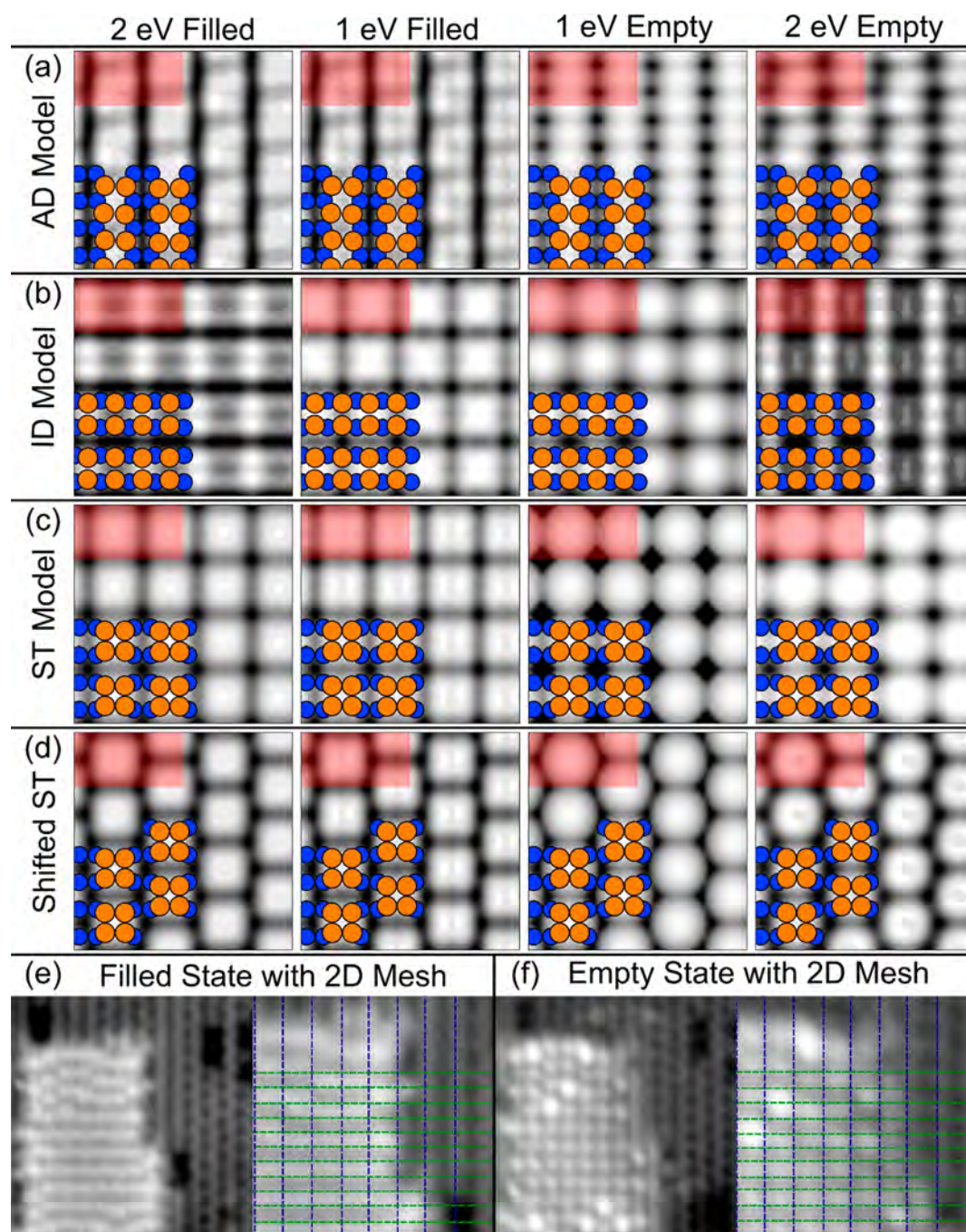


**Figure 3.** STM simulations based on the Tersoff–Hamann theory. Each simulation displays  $8 \times 4 \times 2$  supercells with orange Ag and blue Si dimer atoms for reference. The red box covers the  $4 \times 2$  supercell that tiles the image. (a) Ag dimer model, (b) inequivalent dimer model, (c) square tetramer model, and (d) half-cell shifted square tetramer model. (e,f) Filled- and empty-state STM images of 0.15 ML of Ag on Si(001). Images were collected at 140 K,  $-3.0$  V (filled) and  $+3.9$  V (empty), 10 pA and  $107 \times 104 \text{ \AA}^2$ . Grid image size is  $64 \times 62 \text{ \AA}^2$ . Green lines are placed over the Si dimer bond along the direction of the dimer row, and blue lines are placed along Si dimer bond. The 2D mesh was reproduced similar to ref 25.

characteristic shape of the simulated STM maxima does not change, just as they do not change in STM images. Additionally, the adsorption energy,  $E_{\text{ML}/\text{Ag}}$ , as well as bond lengths and angles of the shifted ST phase do not differ significantly from the nonshifted ST phase ( $\Delta E_{\text{ML}/\text{Ag}} < 4$  meV).

Another type of disorder observed on the Ag/Si(001) surface is shown in Figure 5. From coverages as low as 0.15 ML, local areas on Ag films develop extended bright streaks

that run along, or at a  $45^\circ$  to, the Si dimer row. The proportion of the Ag films covered by these streaks as well as the size of these streaks, increases with increasing Ag coverage, as shown in Figure 5a,b. The smallest resolvable part, which we assign as a Ag interstitial, is visible twice in the Figure 5a inset.

This assignment is supported by the ST model, in which an additional Ag atom is placed in the pedestal site in between four Ag tetramers. Figure 5c,d demonstrates the structural change after DFT relaxation. The STM simulation in Figure 5e

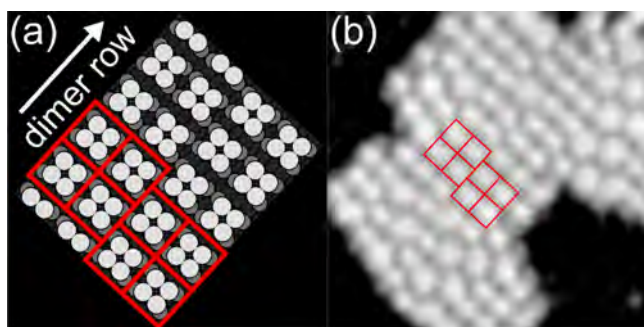


**Figure 4.** Local checkerboard disorder on the Si(001)-Ag( $2 \times 2$ ) reconstruction. (a) Schematic diagram displaying a half-cell shifted dimer row. Red boxes enclose Ag tetramers and correspond to maxima in the STM image. (b) Filled-state STM image of 0.45 ML of Ag on Si(001). Recorded at 140 K,  $-2.5$  V, 20 pA, and  $100 \times 100 \text{ \AA}^2$ . Red boxes enclose STM maxima and highlight the domain between two ( $2 \times 2$ )-Ag domains.

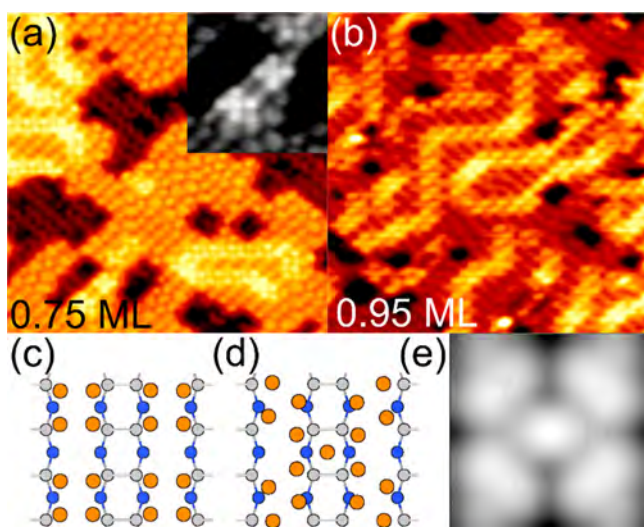


**Figure 5.** X-type defect on the Si(001)-Ag( $2 \times 2$ ) reconstruction. (a,b) STM images showing coverages of 0.75 and 0.95 ML of Ag on Si(001) with a larger proportion of defects on the 0.95 ML surface. The inset in panel a provides an enhanced view of single X-type defects. (c,d) The DFT relaxed structures before and after adding an additional Ag atom in the middle of four  $2 \times 2$  regions. Panel (e) is a filled-state STM simulation of the structure in panel (d). Images were recorded at 140 K,  $-2.5$  V, 20 pA, and  $212 \times 212 \text{ \AA}^2$  for panel a and  $-2.1$  V, 50 pA, and  $209 \times 209 \text{ \AA}^2$  for panel b.

is also able to reproduce the characteristic four-lobed X shape. The additional Ag atom adsorbs with an energy of 3.81 eV, a value much larger than the ML adsorption energy of 2.43 eV, suggesting that this 17/16 ML structure is highly favorable. The transformation from a square shaped tetramer to a diamond shaped tetramer is particularly interesting, as the tetramers retain similar Ag–Ag and Ag–Si interactions while maximizing Ag–Ag interaction to the interstitial Ag atom. The average Ag–Ag distance of 2.84 Å and Ag–Si distance of 2.47 Å among diamond tetramers is very close to the original distances of the ST model. The 4-fold coordinated center Ag atom has slightly larger Ag–Ag and Si–Ag distances of 2.99 and 2.92 Å, respectively. Additionally, the Si(001) layer underneath does not significantly change in Si–Si bond distance or buckling angle, supporting the notion that the same Si–Ag interaction is kept. In the X-type defect, the Ag

tetramers start to approximate a close packed Ag plane. This could be one possible explanation for the experimental observations that 3D islands of Ag on Si(001) were found to have the Ag(111) plane parallel to the Si(001) surface.<sup>9,14,18,44</sup>

**Bias Dependent Contrast Reversal of Ag Films.** The height of Ag films displays a surprisingly strong dependence on the scanning bias. At sufficiently low positive biases (corresponding to empty states near the Fermi level), STM scans register Ag films as a depressed feature relative to the Si(001) surface in adjacent areas. Figure 6a–c demonstrates this bias dependence. Multibias scans of the same region at  $\pm 2.5$  V place a Ag film above the Si(001) surface. At +1.9 V however, the STM scan shows a striking color contrast reversal. The Ag film has a negative height despite being topographically higher than the Si(001) surface. Similar phenomena have been observed on Si substrates (Br/Si(111)<sup>45</sup> and H/Si(001)<sup>46</sup>) and with other metallic films (Au/SrTiO<sub>3</sub>(001)<sup>47</sup>).

Negative Ag film height suggests that there is a high availability of Si(001) surface states relative to Ag states for tunneling. The projected density of states (PDOS) of the ST model provide a clear explanation for this effect. The calculated density of states (DOS) of the ST model and clean Si(001) surface are displayed in Figure 6d with a PDOS zoomed in view around the Fermi level in Figure 6e. The Si(001) PDOS peak at  $\sim 0.9$  eV corresponds to the empty dangling bond state on down dimer atoms. The disappearance of that peak in the ST PDOS suggests the disappearance of the empty dangling bond state and Ag–Si bond formation. As expected, there are very few Ag states available from the Fermi energy to  $\sim 1.2$  eV above the Fermi energy. Therefore, the STM scan in Figure 6b is caused by the high availability of surrounding dangling bond states versus the low availability of Ag states. Note that the highly doped Si sample and the underestimated band gap by the GGA functional only allows for qualitative comparison. The scanning bias does not exactly reflect the position on the DOS. Given that the experimental band gap of Si is  $\sim 1.1$  eV, it is reasonable to expect a shift of at least 0.5 eV (since the GGA band gap is roughly half of the experimental value). PDOS of the AD and ID models are discussed in section S2 of the Supporting Information.

**Coverage Dependent Si–Ag Interaction.** The buckled Si dimers change after DFT relaxation of the ST model. The longer Si dimer bond length ( $\sim 2.44$  Å) and decreased Si dimer angle ( $\sim 0.6^\circ$ ) are similar to the bond length and angle in the H/Si(001)-( $2 \times 1$ ) system<sup>46,48,49</sup> and therefore suggest a comparable electronic interaction. Specifically, this suggests the formation of a covalent bond between Si (3p orbital) and Ag (5s, 4p, and 4d orbitals). The disappearing dangling bond state in Figure 6e also suggests this bond formation. Electron localization function (ELF) plots were calculated for Si(001)-c( $4 \times 2$ ) and the ST model in order to visualize this covalent bond. On the c( $4 \times 2$ ) reconstruction (Figure 7a), the filled dangling bond states over the top dimer atoms are visible as protruding lobes. The  $sp^3$  character of the up dimer atoms and the  $sp^2$  character of the down dimer atoms are clearly shown. The ELF plot of the ST model (Figure 7b) displays all Si dimers with  $sp^3$  character. The lobe located in between the Ag and Si atoms shows covalent bond formation. The small Ag–Si lobes signify that those electrons are less localized than in Si–Si bonds.

Weak covalent bond formation on Ag/Si(001) has been previously predicted. Core level photoemission,<sup>50</sup> ARPES,<sup>41</sup>

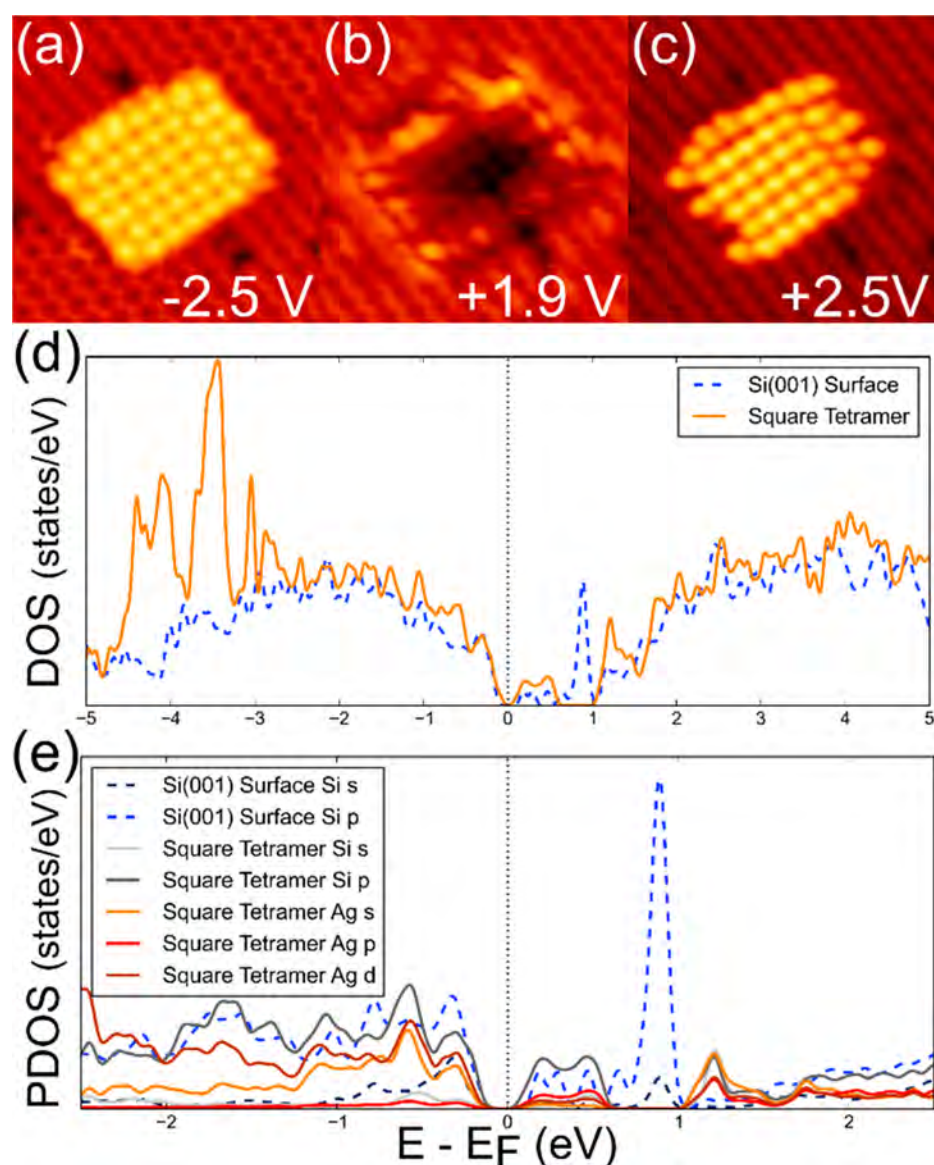


**Figure 6.** (a–c) Multibias STM images of 0.15 ML of Ag on Si(001). The same Ag film reveals low Ag DOS at low positive bias. Scanning parameters were +2.5, +1.9, and –2.5 V, respectively, with 15 pA,  $98 \times 98 \text{ \AA}^2$ , and 81 K. (d) Total DOS of the Si(001)- $c(4 \times 2)$  surface and the ST model. (e) PDOS of the top layers (surface Si and Ag) of both surfaces as in panel (d).

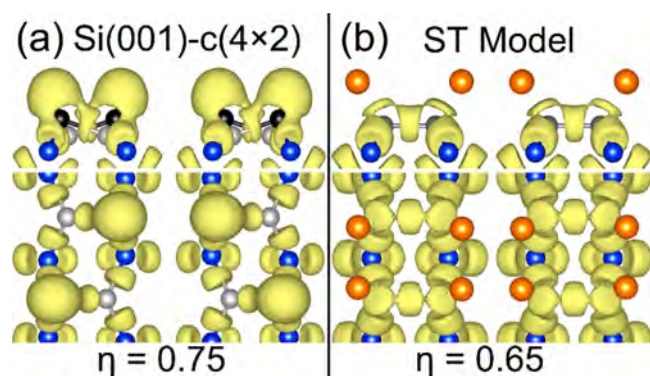


**Figure 7.** Electron localization function isosurface plots of (a) the clean Si(001)- $c(4 \times 2)$  surface and (b) ST model.  $\eta = 0.5$  corresponds to a uniform electron gas, and  $\eta = 1$  corresponds to a fully localized electron. The top two Si layers are shown.

and surface reflectance spectroscopy (along with differential reflectance)<sup>51–53</sup> suggest that the ML structure is semi-conducting and contains some covalent bonding. Borensztein and Alameh<sup>51–53</sup> also suggested that at 1 ML, each Ag adatom is bound to one Si atom because of similar reflectance behavior between Ag/Si(001) and Ag/Si(111). The ST model shares a number of similarities with the Ag/Si(111) monolayer structure. The inequivalent triangle (IET) model (Si(111)- $(\sqrt{3} \times \sqrt{3})R^{30}\text{-Ag}$ )<sup>54</sup> features Ag trimers with Ag coordinated to two Ag atoms and one Si atom. Si at the surface forms Si trimers and additionally bonds with one Ag atom in an attempt to saturate all dangling bonds. The ST models shows a similar scheme where every Ag adatom is coordinated to two Ag atoms and bonds to one Si dimer atom.

From ML simulations alone, it is not clear to what extent Si buckling (or unbuckling) plays in the adsorption of Ag on Si(001) and how Ag–Ag interaction affects the formation of the ML structure. To provide further insight, single site Ag adsorption on the  $c(4 \times 2)$  reconstruction was performed.

This allowed for the study of Ag–Si interaction without additional Ag–Ag interaction. Adsorption sites are displayed in Figure 8, and relaxed values are listed in the sequence of

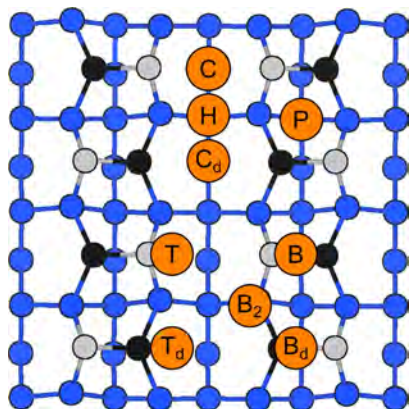


**Figure 8.** Ag atom adsorption sites on the  $c(4 \times 2)$  reconstruction. Simulations were done on a  $(4 \times 2)$  supercell (eight Si atoms at the topmost layer), producing a coverage of  $\Theta_{\text{Ag}} = 1/8$  ML.

decreasing adsorption energy in Table 2. The comparison with LDA energies (and energies from Kong et al.<sup>27</sup>) are discussed in section S3 of the Supporting Information. All adsorption energies were calculated from eq 3. Up and down dimer sites for the cave (C), bridge (B), and near dimer (T) sites are distinguished with a subscript “d” to indicate the down dimer position.

$$E_{\text{Ad}} = -(E_{\text{Ag+Si surf}} - E_{\text{Si surf}} - E_{\text{Ag}}) \quad (3)$$

When Ag is coordinated between two or more Si atoms (C, B<sub>2</sub>, P, B<sub>d</sub> and C<sub>d</sub>) the distance between Ag and Si ( $d_{\text{Ag-Si}}$ ) is larger than that when Ag is coordinated to one Si atom (T<sub>d</sub>, T, and B). This suggests a more local interaction in the one-to-one sites. Most Si dimer bond lengths changes were  $<0.05$  Å. Since 0.05 Å is the difference between the buckled and H terminated dimer,<sup>48,49</sup> we can conclude that single Ag adsorption does not break the Si dimer  $\pi$  bond, except in the C and C<sub>d</sub> sites where two-to-one covalent interaction develops. CDD and ELF plots in section S3.2 of the Supporting Information show evidence of this covalent interaction.

The buckling angle ( $\theta_{\text{Si-Si}}$ ) deviates significantly from the clean surface value of 19.4°. Buckling is responsible for charge transfer between the dangling bond states,<sup>55,56</sup> and alternating buckling along the Si dimer row is a mechanism to reduce surface stress.<sup>57,58</sup> Therefore, observing changes in these parameters indicate electronic rearrangement between dangling bonds states and a competition between surface stress

and electronic interaction. Upon Ag adsorption, the buckling angle decreases. The decrease is larger when only one dimer is involved, suggesting increased electron transfer from the up dimer atom. In the B<sub>2</sub> and the T<sub>d</sub> sites, a dimer switches its buckling orientation, indicating that the increase in energy from the electronic interaction surpasses the increased energy from stress. Unaffected dimers typically saw angle changes less than 1°.

The most stable sites (C, B<sub>2</sub>, and P) interact with two or four Si atoms across two dimer pairs and have relatively small angle changes. Less stable sites (B<sub>d</sub>, T<sub>d</sub>, T, and B) interact with one or two Si atoms across a single dimer and generally feature much large angle changes. The C<sub>d</sub> and H sites seem to be exceptions to these trends; however, their small adsorption energies are simply because of their location far away from up Si dimer atoms.

While we find that the C adsorption site is the most stable site similar to Kong et al.,<sup>27</sup> we can clearly state that it is the up dimer cave site and not the down dimer cave site responsible for the stability. The results of Kong et al.<sup>27</sup> were on the  $p(2 \times 2)$  reconstruction and that C site includes one up and one down dimer. Previous claims that this site is ideal due to the inherent Si–Ag–Si bond distance<sup>50</sup> are not incorrect. However, the significant electronic interaction with the up dimer’s filled dangling bonds and minimal increase in stress provides a more complete description. Ag adsorption at all other sites have not been experimentally observed. This can most likely be attributed to highly mobile Ag adatoms and/or by the preference of Ag to form larger clusters when possible.

One surprising result is that the energies in Table 2 do not correlate with the experimental energies of Starr et al.<sup>26</sup> The heat of adsorption for  $\Theta_{\text{Ag}} = 1/8$  is  $\sim 3.47$  eV, a value larger than any calculation presented. Adsorption at step edges or defect sites could be possible explanations for this difference. In situ RT-STM experiments<sup>16,17</sup> have shown that during Ag deposition, C-type defects (dissociated H<sub>2</sub>O molecules) trap Ag atoms. Additionally, formation of Ag clusters, such as dimer and tetramers or chains and islands, could also explain this difference in adsorption energy. Further simulations of Ag on more complex Si(001) geometries, such as step edges or C-type defects, can provide reference data for the in situ experiments. This may be a challenging task given that unit cells would have to be quite large and that C-type defects can transform into several different structures at RT.<sup>59</sup>

From the simulations at low coverages and at 1 ML coverage, it is clear that Ag/Si(001) behaves very differently depending on the Ag coverage. At low coverages, Ag adatoms prefer to have a 2-fold coordinated adsorption site with electronic interaction from up Si dimer atoms. At 1 ML, Ag–Ag interaction is clearly preferred, as the ST model features a cluster of four Ag adatoms. Si atoms do not break their dimer

**Table 2.** Computed Ag Adsorption Values from DFT Simulations on the Si(001)- $c(4 \times 2)$  Reconstruction

site	C (cave)	B <sub>2</sub> (bridge 2)	P (pedestal)	B <sub>d</sub> (bridge)	T <sub>d</sub> (near dimer)	T (near dimer)	B (bridge)	C <sub>d</sub> (cave)	H (hallow)
affected dimers	2	2	2	1	1	1	1	2	4
Ag–Si coordination	2	2	4	2	1	1	1	2	4
$E_{\text{ad}}$ (eV)	2.26	2.17	2.01	1.88	1.85	1.78	1.76	1.75	1.37
$d_{\text{Si-Ag}}$ (Å)	2.56	2.52	2.60/2.97	2.48/2.59	2.39	2.39	2.38	2.74	3.36
$\Delta d_{\text{Si-Si}}$ (Å)	0.06	−0.005	−0.002	−0.003	0.03	0.01	−0.008	0.05	0.02
$\Delta \theta_{\text{Si-Si}}$ (deg)	−5.67	−8.56 <sup>a</sup>	−0.95	−15.00	−21.4	−10.2	−7.14	−4.20	−1.20

<sup>a</sup>In the B<sub>2</sub> site, both Si dimers buckled in the same direction.

bond, but rather try to saturate their dangling bond states and act in an  $sp^3$  hybridization scheme similar to bulk Si. From these trends, we can conclude that Si and Ag both prefer to remain segregated, primarily maximizing Si–Si and Ag–Ag interaction first and only secondarily choosing to have Ag–Si interaction.

## CONCLUSION

DFT and LT-STM agree on the ST model as the  $(2 \times 2)$ -Ag ML structure. The notion of a Ag dimer covered monolayer on Si(001) was proven inconsistent with STM data through DFT simulations. The ST model best matched STM images and the more subtle features therein, namely the checkerboard disorder, the X-type defect, and the bias dependence of the measured Ag height. This new model of the  $(2 \times 2)$ -Ag structure creates many new avenues of research to be explored. A better understanding of the unwetting phenomena or simply the transition from the 2D layer to 3D islands is the next step toward fully understanding the Ag/Si(001) system at RT.

## METHODS

**Theory.** DFT calculations were carried out in the Vienna Ab initio Simulations Package (VASP).<sup>60</sup> Projector augmented-wave (PAW) potentials<sup>61,62</sup> were used along with the exchange-correlation functional of Perdew–Burke–Ernzerhof in the generalized gradient approximation (PBE-GGA)<sup>63</sup> and the local density approximation (LDA).<sup>64</sup> Presented geometries and values stem from simulations with PBE-GGA functionals, as they generally provide a more realistic approximation of adsorption energies over LDA functionals. Simulations with LDA functionals are included in section S3 of the Supporting Information. Si(001) slabs ( $2 \times 2$ ,  $4 \times 2$ , and  $4 \times 4$ ) were created with either 8 or 10 Si layers and passivated with terminating H groups at the bottom. A vacuum space of  $\sim 15$  Å was used. A kinetic energy cut-off of 500 eV and a k-point sampling grid of  $4 \times 4 \times 1$  under the Monkhorst–Pack scheme<sup>65</sup> were used. The ionic force relaxation threshold was  $1 \times 10^{-5}$  eV/Å, and the electronic self-consistent threshold was  $1 \times 10^{-6}$  eV. Si(001) slabs were relaxed with the top six Si layers free, and all subsequent calculations involving Ag adsorption were relaxed with Ag and the top two Si layers free. The STM simulations were conducted using an algorithm based on the Tersoff–Hamann method.<sup>43</sup>

Sensitivity tests were conducted to ensure that relaxing 2 Si layers during Ag adsorption was sufficient. No significant change in adsorption energy ( $<10$  meV) was found when varying the number of Si layers in the slab (6, 8, or 10 layers) and varying the numbers of free Si layers (2, 3, 4, or 6 layers) during adsorption. Sensitivity tests were also conducted to validate the chosen force and electronic self-consistency threshold values. Percent deviations less than 1% were found in the adsorption energy and atomic distances when varying the force threshold from  $1 \times 10^{-3}$  to  $1 \times 10^{-5}$  eV/Å and the electronic threshold from  $1 \times 10^{-4}$  to  $1 \times 10^{-8}$  eV. Additional details can be found in section S4 of the Supporting Information.

**Experiment.** Experiments were carried out in a cryogen-free closed-cycle STM (RHK PanScan Freedom) system, with a base pressure of  $\sim 1.0 \times 10^{-10}$  Torr. Samples of Si(001) were cut from a phosphorus-doped wafer (resistivity of 0.01–0.02  $\Omega^*cm$ ) or an arsenic-doped wafer (resistivity of 0.001–0.005  $\Omega^*cm$ ). In vacuum, Si(001) surfaces were cleaned by repeated flashes to 1373 K. To prepare Ag films, the clean Si(001) sample was held at room temperature for silver deposition from a coiled tungsten filament by direct-current heating. Subsequently, the sample was transferred into the precooled STM for examination at a stable temperature between 15 and 300 K, as regulated by a PID-based temperature controller (Lakeshore 325). The deposition rates of silver were monitored by an in situ quartz crystal microbalance to be as stable as 0.15 ML/min (1 ML =  $6.78 \times 10^{14}$   $cm^{-2}$ ) during the course of deposition, in agreement with what was derived from STM images. All STM images

were recorded by a platinum/iridium tip in the constant-current mode and processed with WSxM.<sup>66</sup> Imaging biases in figures refer to silicon sample bias.

## ASSOCIATED CONTENT

### Supporting Information

The Supporting Information is available free of charge on the ACS Publications website at DOI: 10.1021/acsaelm.8b00058.

S1. Ag monolayer simulations on the Si(001)- $p(2 \times 2)$  reconstruction; S2. Projected density of states of other  $(2 \times 2)$  Ag models; S3. Details of single site Ag adsorption on Si(001)- $c(4 \times 2)$ ; S4. Sensitivity to relaxation and threshold parameters (PDF)

## AUTHOR INFORMATION

### Corresponding Author

\*E-mail: chandraveer.singh@utoronto.ca.

### ORCID

William S. Huxter: 0000-0003-1170-4241

Kai Huang: 0000-0001-8907-4441

Jun Nogami: 0000-0002-4758-0546

Chandra Veer Singh: 0000-0002-6644-0178

### Notes

The authors declare no competing financial interest.

## ACKNOWLEDGMENTS

This research was enabled in part by support provided by the Natural Sciences and Engineering Research Council of Canada (NSERC), the Hart Professorship, and the University of Toronto. Computations were conducted through the Compute Canada facilities, namely Cedar and SciNet GPC. SciNet is funded by the Canada Foundation for Innovation, NSERC, the Government of Ontario, Fed Dev Ontario, and the University of Toronto.

## REFERENCES

- (1) Le Lay, G. Physics and Electronics of the Noble-Metal/Elemental-Semiconductor Interface Formation: A Status Report. *Surf. Sci.* **1983**, *132*, 169–204.
- (2) Hanbücken, M.; Le Lay, G. Formation of Noble-Metal-Si(100) Interfaces. *Surf. Sci.* **1986**, *168*, 122–132.
- (3) Vogt, P.; De Padova, P.; Quaresima, C.; Avila, J.; Frantzeskakis, E.; Asensio, M. C.; Resta, A.; Ealet, B.; Le Lay, G. Silicene: Compelling Experimental Evidence for Graphene like Two-Dimensional Silicon. *Phys. Rev. Lett.* **2012**, *108*, 155501.
- (4) Feng, B.; Ding, Z.; Meng, S.; Yao, Y.; He, X.; Cheng, P.; Chen, L.; Wu, K. Evidence of Silicene in Honeycomb Structures of Silicon on Ag(111). *Nano Lett.* **2012**, *12*, 3507–3511.
- (5) Kiraly, B.; Iski, E. V.; Mannix, A. J.; Fisher, B. L.; Hersam, M. C.; Guisinger, N. P. Solid-Source Growth and Atomic-Scale Characterization of Graphene on Ag(111). *Nat. Commun.* **2013**, *4*, 2804.
- (6) Mannix, A. J.; Zhou, X.-F.; Kiraly, B.; Wood, J. D.; Alducin, D.; Myers, B. D.; Liu, X.; Fisher, B. L.; Santiago, U.; Guest, J. R.; Yacaman, M. J.; Ponce, A.; Oganov, A. R.; Hersam, M. C.; Guisinger, N. P. Synthesis of Borophenes: Anisotropic, Two-Dimensional Boron Polymorphs. *Science* **2015**, *350*, 1513.
- (7) Tao, L.; Cinquanta, E.; Chiappe, D.; Grazianetti, C.; Fanciulli, M.; Dubey, M.; Molle, A.; Akinwande, D. Silicene Field-Effect Transistors Operating at Room Temperature. *Nat. Nanotechnol.* **2015**, *10*, 227–231.
- (8) Samsavar, A.; Hirschorn, E. S.; Leible, F. M.; Chiang, T.-C. Scanning-Tunneling Microscopy Studies of Ag on Si(100)- $(2 \times 1)$ . *Phys. Rev. Lett.* **1989**, *63*, 2830–2833.

- (9) Hashizume, T.; Hamers, R. J.; Demuth, J. E.; Markert, K.; Sakurai, T. Initial Stage Deposition of Ag on the Si(100) $2 \times 1$  Surface Studied by Scanning Tunneling Microscopy. *J. Vac. Sci. Technol., A* **1990**, *8*, 249–250.
- (10) Brodde, A.; Badt, D.; Tosch, S.; Neddermeyer, H. The Growth of Ag Films on Si(100). *J. Vac. Sci. Technol., A* **1990**, *8*, 251–254.
- (11) Lin, X. F.; Wan, K. J.; Nogami, J. Ag on the Si(001) Surface: Growth of the First Monolayer at Room Temperature. *Phys. Rev. B: Condens. Matter Mater. Phys.* **1993**, *47*, 13491.
- (12) Ichinokawa, T.; Itoh, H.; Schmid, A.; Winau, D.; Kirschner, J. Scanning Tunneling Microscopic Studies of Surface Reconstructed Structures for Metals/Si(100) Systems. *Ultramicroscopy* **1994**, *54*, 116–124.
- (13) Winau, D.; Itoh, H.; Schmid, A. K.; Ichinokawa, T. Reconstructions and Growth of Ag on Si(001)( $2 \times 1$ ). *Surf. Sci.* **1994**, *303*, 139–145.
- (14) Winau, D.; Itoh, H.; Schmid, A. K.; Ichinokawa, T. Ag on Si(001)( $2 \times 1$ ) Formation of a  $2 \times 3$  Superstructure. *J. Vac. Sci. Technol., B: Microelectron. Process. Phenom.* **1994**, *12*, 2082–2085.
- (15) Glueckstein, J. C.; Evans, M. M. R.; Nogami, J. Surface Unwetting During Growth of Ag on Si(001). *Phys. Rev. B: Condens. Matter Mater. Phys.* **1996**, *54*, R11066.
- (16) Kocán, P.; Sobotík, P.; Ošťádal, I. Role of Surface Defects in Room-Temperature Growth of Metals on Si(100) $2 \times 1$ . *Czech. J. Phys.* **2006**, *56*, 27–32.
- (17) Kocán, P.; Ošťádal, I.; Sobotík, P. Growth of Silver Structure on Silicon Surfaces Observed in vivo by Scanning Tunneling Microscopy. *Surf. Sci.* **2006**, *600*, 3928–3931.
- (18) Takeuchi, O.; Kageshima, M.; Sakama, H.; Kawazu, A. Atomically Resolved Nucleation and Initial Growth of a Ag Three-Dimensional Island on Si(001) Substrate. *Phys. Rev. B: Condens. Matter Mater. Phys.* **2011**, *83*, 205433.
- (19) Lin, X. F.; Wan, K. J.; Nogami, J. Ag on Si(001): Growth Behavior of the Annealed Surface. *Phys. Rev. B: Condens. Matter Mater. Phys.* **1993**, *47*, 10947.
- (20) Lin, X. F.; Wan, K. J.; Nogami, J. Surface Reconstruction in the Ag/Si(001) System. *Phys. Rev. B: Condens. Matter Mater. Phys.* **1994**, *49*, 7385.
- (21) Shivaprasad, S. M.; Abukawa, T.; Yeom, H. W.; Nakamura, M.; Suzuki, S.; Sato, S.; Sakamoto, K.; Sakamoto, T.; Kono, S. Ag Adsorption on a Single Domain Si(001) $2 \times 1$  Surface Studied by Electron and Photoelectron Diffraction. *Surf. Sci.* **1995**, *344*, L1245–L1251.
- (22) Alekseev, A. A.; Kotlyar, V. G.; Utas, O. A.; Gruznev, D. V.; Matetskiy, A. V.; Zotov, A. V.; Saranin, A. A. Atomic and Electronic Structures of Ag/Si(100)-c( $6 \times 2$ ) Surface: A First-Principles Study. *Surf. Sci.* **2010**, *604*, 1400.
- (23) Zhang, X.; Cai, Y.; Chen, F.; Kong, H.; OuYang, H.; Liu, S.; Liu, X.; Wang, L. Ag-Induced Si(100) Reconstruction: Si(100)-( $2\sqrt{2} \times 2\sqrt{2}$ )R<sup>o</sup>45-Ag. *Phys. Rev. B: Condens. Matter Mater. Phys.* **2011**, *84*, 153411.
- (24) Park, N. G.; Kim, Y. W.; Cho, W. S.; Kim, J. Y.; Choi, D. S.; Jeong, K.; Chae, K. H.; Whang, C. N. Atomic Structure of Two-Dimensional Ag Layer Grown on Si(001)-( $2 \times 1$ ) at Room Temperature. *Surf. Sci.* **1998**, *414*, L945–L950.
- (25) Huang, K.; Huxter, W. S.; Singh, C. V.; Nogami, J. Identification of Tetramers in Silver Films Grown on the Si(001) Surface at Room Temperature. *J. Phys. Chem. Lett.* **2018**, *9*, 6275–6279.
- (26) Starr, D. E.; Ranney, J. T.; Larsen, J. H.; Musgrove, J. E.; Campbell, C. T. Measurement of the Energetics of Metal Film Growth on a Semiconductor: Ag/Si(00)-( $2 \times 1$ ). *Phys. Rev. Lett.* **2001**, *87*, 106102.
- (27) Kong, K. J.; Yeom, H. W.; Ahn, D.; Yi, H.; Yu, B. D. Ab initio Study of Adsorption and Diffusion of Ag Atoms on a Si(001) Surface. *Phys. Rev. B: Condens. Matter Mater. Phys.* **2003**, *67*, 235328.
- (28) Ramstad, A.; Brocks, G.; Kelly, P. J. Theoretical Study of the Si(001) Surface Reconstruction. *Phys. Rev. B: Condens. Matter Mater. Phys.* **1995**, *51*, 14504–14325.
- (29) Zhou, R.-H.; Cao, P.-L.; Lee, L.-Q. Cluster Models Study of Ag Bonding, Migration and Interaction on Si(100)- $2 \times 1$ . *Surf. Sci. Lett.* **1993**, *290*, L649–L654.
- (30) Okon, J. C.; Joachim, C. Chemisorption of a Ag atom on a Si(100)  $2 \times 1$  Surface: Local Surface Deformation. *Surf. Sci.* **1997**, *376*, L409–L413.
- (31) Mazzone, A. M. LDA and Molecular Dynamics Determination of Ag Deposition onto (100) Surfaces in Silicon. *Thin Solid Films* **2003**, *428*, 139–143.
- (32) Mazzone, A. M. Ag Deposited onto the (100) Surface in Silicon Studied by Density Functional Theory and Classical Molecular Dynamics. *Eur. Phys. J. B* **2003**, *35*, 517–524.
- (33) Wei, S.-Y.; Li, W.; Zhang, F.; Zhao, X. Adsorption of Ag on Si(100) Surface. *Phys. B* **2007**, *390*, 191–195.
- (34) Kim, S.-K.; Kim, J.-S.; Lee, G.; Nogami, J.; Kong, K.-J.; Yu, B. D.; Ahn, D. Electronic Structure of p( $2 \times 3$ ) Ag Films on Si(100). *J. Korean Phys. Soc.* **2013**, *62*, 86–91.
- (35) Wolkow, R. A. Direct Observation of an Increase in Buckled Dimers on Si(001) at Low Temperature. *Phys. Rev. Lett.* **1992**, *68*, 2636–2639.
- (36) Guo, C.-S.; Hermann, K.; Zhao, Y. Dynamics and Energetics of Reconstruction at the Si(100) Surface. *J. Phys. Chem. C* **2014**, *118*, 25614–25619.
- (37) Neergaard Waltenburg, H.; Yates, J. T. Surface Chemistry of Silicon. *Chem. Rev.* **1995**, *95*, 1589–1673.
- (38) McNab, I. R.; Polanyi, J. C. Imprinting Atomic and Molecular Patterns. *Front. Nanosci.* **2011**, *2*, 79–120.
- (39) Abukawa, T.; Kono, S. Photoelectron Diffraction Study of Si(001) $2 \times 1$ -K Surface: Existence of a Potassium Double Layer. *Phys. Rev. B: Condens. Matter Mater. Phys.* **1988**, *37*, 9097–9099.
- (40) Matsuda, I.; Yeom, H. W.; Tono, K.; Ohta, T. Angle-Resolved Photoemission Study of Electron Structure Development During Ag Growth on the Si(001) Surface. *Surf. Sci.* **1999**, *438*, 231–236.
- (41) Yeom, H. W.; Matsuda, I.; Tono, K.; Ohta, T. Electronic Surface of the Si(001)c( $6 \times 2$ )-Ag Surface Studied by Angle-Resolved Photoelectron Spectroscopy using Synchrotron Radiation. *Phys. Rev. B: Condens. Matter Mater. Phys.* **1998**, *57*, 3949–3954.
- (42) Matsuda, I.; Yeom, H. W.; Tono, K.; Ohta, T. Electronic Structure of the Si(001) $2 \times 3$ -Ag Surface. *Phys. Rev. B: Condens. Matter Mater. Phys.* **1999**, *59*, 15784–15788.
- (43) Tersoff, J.; Hamann, D. R. Theory of the Scanning Tunneling Microscope. *Phys. Rev. B: Condens. Matter Mater. Phys.* **1985**, *31*, 805.
- (44) Horn-von Hoegen, M.; Schmidt, T.; Meyer, G.; Winau, D.; Rieder, K. H. Lattice Accommodation of low-index planes: Ag(111) on Si(001). *Phys. Rev. B: Condens. Matter Mater. Phys.* **1995**, *52*, 10764–10767.
- (45) Guo, H.; Ji, W.; Polanyi, J. C.; Yang, J. S. Y. Molecular Dynamics of Localized Reaction, Experiment and Theory: Methyl Bromide on Si(111)- $7 \times 7$ . *ACS Nano* **2008**, *2*, 699–706.
- (46) Labidi, H.; Kantorovich, L.; Riedel, D. Atomic-Scale Control of Hydrogen Bonding on a Bare Si(100)- $2 \times 1$  Surface. *Phys. Rev. B: Condens. Matter Mater. Phys.* **2012**, *86*, 165441.
- (47) Silly, F.; Castell, M. R. Bimodal Growth of Au on SrTiO<sub>3</sub>(001). *Phys. Rev. Lett.* **2006**, *96*, 086104.
- (48) Kratzer, P.; Hammer, B.; Nørskov, J. K. Direct Pathway for Sticking/Desorption of H<sub>2</sub> on Si(100). *Phys. Rev. B: Condens. Matter Mater. Phys.* **1995**, *51*, 13432–13440.
- (49) Lauridsen, E. M.; Baker, J.; Nielsen, M.; Feidenhansl, R.; Falkenberg, G.; Bunk, O.; Zeysing, J. H.; Johnson, R. L. Structure Determination of the Si(001)-( $2 \times 1$ )-H Reconstruction by Surface X-ray Diffraction: Weakening of the Dimer Bond by the Addition of Hydrogen. *Surf. Sci.* **2000**, *453*, 18–24.
- (50) Samsavar, A.; Miller, T.; Chiang, T.-C. Determination of the Bonding and Growth of Ag on Si(100)-( $2 \times 1$ ). *Phys. Rev. B: Condens. Matter Mater. Phys.* **1988**, *38*, 9889–9893.
- (51) Borensztein, Y.; Alameh, R. Optical Evidence for Interface Electronic States at Ag/Si Interfaces. *Surf. Sci.* **1992**, *274*, L509–L514.
- (52) Borensztein, Y.; Alameh, R. The Growth on Ag on Si(100)- $2 \times 1$ . *Appl. Surf. Sci.* **1993**, *65–66*, 735–741.

- (53) Borensztein, Y.; Alameh, R.; Roy, M. Sudden Beginning of Metallic Behavior at Ag/Si(100) Interface: A Real-Time Photo-reflectance Spectroscopy Investigation. *Phys. Rev. B: Condens. Matter Mater. Phys.* **1993**, *48*, 14737–14740.
- (54) Aizawa, H.; Tsukada, M.; Sato, N.; Hasegawa, S. Asymmetric Structure of the Si(111)- $\sqrt{3}\times\sqrt{3}$ -Ag Surface. *Surf. Sci.* **1999**, *429*, L509–L514.
- (55) Chadi, D. L. Atomic and Electronic Structures of Reconstructed Si(100) Surfaces. *Phys. Rev. Lett.* **1979**, *43*, 43–47.
- (56) Rohlfing, M.; Krüger, P.; Pollmann, J. Metallic Nature of the Symmetric Dimer Model of Si(001)-(2 × 1). *Phys. Rev. B: Condens. Matter Mater. Phys.* **1995**, *52*, 13753–13756.
- (57) Dąbrowski, J.; Pehlke, E.; Scheffler, M. Calculation of the Surface Stress Anisotropy for the Buckled Si(001)(1 × 2) and p(2 × 2) Surfaces. *Phys. Rev. B: Condens. Matter Mater. Phys.* **1994**, *49*, 4790–4793.
- (58) van Heys, J.; Pehlke, E. Surface Stress of Partially H-Covered Si(001) Surfaces. *Phys. Rev. B: Condens. Matter Mater. Phys.* **2005**, *72*, 125351.
- (59) Sobotik, P.; Ošťádal, I. Transformation of C-Type Defects on Si(100)-2 × 1 Surface at Room Temperature – STM/STS Study. *Surf. Sci.* **2008**, *602*, 2835–2839.
- (60) Kresse, G.; Furthmüller, J. Efficient Iterative Schemes for ab initio Total-Energy Calculations using a Plane-Wave Basis set. *Phys. Rev. B: Condens. Matter Mater. Phys.* **1996**, *54*, 11169.
- (61) Blöchl, P. E. Projector Augmented-Wave Method. *Phys. Rev. B: Condens. Matter Mater. Phys.* **1994**, *50*, 17953–17979.
- (62) Kresse, G.; Joubert, D. From Ultrasoft Pseudopotentials to the Projector Augmented-Wave Method. *Phys. Rev. B: Condens. Matter Mater. Phys.* **1999**, *59*, 1758.
- (63) Perdew, J. P.; Burke, K.; Ernzerhof, M. Generalized Gradient Approximation made Simple. *Phys. Rev. Lett.* **1996**, *77*, 3865.
- (64) Perdew, J. P.; Zunger, A. Self-Interaction Correction to Density-Functional Approximations for Many-Electron Systems. *Phys. Rev. B: Condens. Matter Mater. Phys.* **1981**, *23*, 5048.
- (65) Monkhorst, H.; Pack, J. Special Points for Brillouin-Zone Integrations. *Phys. Rev. B: Condens. Matter Mater. Phys.* **1976**, *13*, 5188–5192.
- (66) Horcas, I.; Fernández, R.; Gómez-Rodríguez, J. M.; Colchero, J.; Gómez-Herrero, J.; Baro, A. M. WSXM: A Software for Scanning Probe Microscopy and a Tool for Nanotechnology. *Rev. Sci. Instrum.* **2007**, *78*, 013705.